Synthesis, Modelling, and Antimitotic Properties of Tricyclic Systems Characterised by a 2-(5-Phenyl-1H-pyrrol-3-yl)-1,3,4-oxadiazole Moiety

Gérard A. Pinna,[b] Gabriele Murineddu,[b] Caterina Murruzzu,[b] Valentina Zuco,[c] Franco Zunino,[c] Graziella Cappelletti,[d] Roberto Artali,[a] Giorgio Cignarella,[a] Lucrezia Solano,[a] and Stefania Villa*[a]

Interesting antitumour activity was observed in a series of tricyclic compounds characterised by the presence of a 2-(1H-pyrrol-3-yl)-1,3,4-oxadiazole moiety that is variously substituted. Their synthesis and antiproliferative activity toward a panel of human tumour cell lines is described. The two most interesting compounds were selected for further evaluation to elucidate their possible mechanism of action. Analysis of cell cycle, tubulin polymerisation, modulation of mitotic markers of the M phase, and apoptosis showed that antimitotic activity is the primary mechanism of the cytotoxic effects of these compounds. Experiments performed on isolated tubulin confirmed that the compounds act by inducing tubulin polymerisation, like taxanes. The binding model against tubulin was also examined by molecular modelling and docking. The results support the proposed binding model, which is able to explain the activity of the oxadiazole derivatives on the basis of their docking energy.

Introduction

Microtubules are protein polymers that are involved in many physiological processes, especially mitosis and cell division, and are formed by α-tubulin and β-tubulin heterodimers.[1] Interference with the dynamics of microtubules polymerisation and depolymerisation, and consequently with cell division, has been proven to be clinically useful for designing anticancer agents. The antimitotic agents have been grouped in three distinct classes on the basis of their different mechanisms of action and binding sites on tubulin. The vinca alkaloids (vincristine, vinblastine, vindesine, and vinorelbine) are microtubule polymerisation inhibitors or depolymerisers and are important in the treatment of leukaemias, lymphomas, small-cell lung cancer and other cancers.[1–3] The colchicines are microtubule polymerisation inhibitors that are similar to the vinca alkaloids,[4] but with a different binding site and depolymerisation mechanism. Taxanes and epothilones[5] inhibit the microtubules function by inducing their polymerisation. Paclitaxel and docetaxel, which belong to the latter class, are two of the most important anticancer drugs today and are widely used as components of chemotherapies for ovarian and breast carcinomas. In addition, they show efficacy against a large number of other solid tumours including carcinomas of the lung, head, neck, bladder and oesophagus.[6] The crystallographic structure of tubulin[7] complexed with paclitaxel has allowed the characterisation of its binding site, which partially overlaps with that of other compounds such as epothilones and eleutherobin.[8,9] In previous studies we discovered interesting antitumour activity in a series of compounds that are characterised by the presence of a pyrrole oxadiazole system that was variously substituted. The compounds were tested in vitro by NCI against 60 tumour cell lines that were derived from nine cancer cell types. The best activity was found for 2-phenyl-5-(5-phenyl-1H-pyrrol-3-yl)-[1,3,4]oxadiazole (GI$_{50}$ = 85.1 μM expressed as a mean), which became our lead compound (A, Figure 1; unpublished data). The insertion of a methyl group at position 3 on the pyrrole ring of the lead compound A brought about a complete loss of antiproliferative activity, possibly due to an unfavoura-
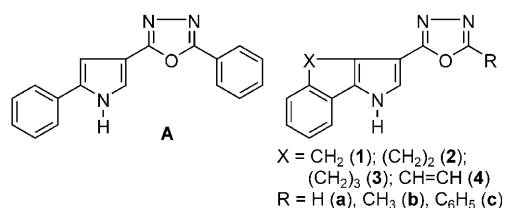

Figure 1. Lead compound and structure optimisation concept.

X = CH$_2$ (**1**); (CH$_2$)$_2$ (**2**); (CH$_2$)$_3$ (**3**); CH=CH (**4**)
R = H (**a**), CH$_3$ (**b**), C$_6$H$_5$ (**c**)

[a] Dr. R. Artali, Prof. G. Cignarella, Dr. L. Solano, Dr. S. Villa
Dipartimento di Scienze Farmaceutiche "P. Pratesi"
Università di Milano, Via Mangiagalli 25, 20133 Milano (Italy)
Fax: (+39) 025 031 9359
E-mail: stefania.villa@unimi.it

[b] Prof. G. A. Pinna, Dr. G. Murineddu, Dr. C. Murruzzu
Dipartimento Farmaco Chimico Tossicologico
Università di Sassari, Via F. Muroni 23, 07100 Sassari (Italy)

[c] Dr. V. Zuco, Dr. F. Zunino
Istituto dei Tumori, Via Venezian 1, 20133 Milano (Italy)

[d] Dr. G. Cappelletti
Dipartimento di Biologia
Università di Milano, Via Celoria 26, 20133 Milano (Italy)

These are not the final page numbers! ↗↗

ble orientation of the molecule with respect to the active site of the receptor. To verify this hypothesis, we planned to tether the configuration of the lead compound by inserting a carbon bridge of different lengths between the phenyl and the pyrrole moieties. In particular, five-, six-, and seven-membered rings were considered, including a benzene ring (compounds **1–4**, Figure 1). The synthesis of derivatives that have the 2-position of oxadiazole unsubstituted (R=H) or methyl substituted (R= CH₃) was also performed. All compounds were evaluated by NCI for their in vitro cytotoxic activity against 60 human tumour cell lines that are derived from nine cancer cell types. The concentrations that inhibited cell growth by 50% (GI$_{50}$, in μM) are reported in Table 1. Based on the preliminary results, the most interesting compounds **1c** and **4c** were selected for further evaluation to understand their possible mechanism of action. In particular, analysis of cell cycle, tubulin polymerisation, modulation of the mitotic markers of M phase, and apoptosis showed that antimitotic activity is the primary mechanism of their cytotoxic effects. The experiment that was performed on isolated tubulin confirmed that the compounds act by inducing tubulin polymerisation, like taxanes. Moreover the tubulin binding mode of oxadiazole derivatives is proposed by molecular modelling and molecular docking investigations.

Results and Discussion

Chemistry

Compounds **7–9** were treated with hydrazine monohydrate to give the corresponding hydrazides, which in turn were condensed with the appropriate orthoesters in DMF at reflux to give the final compounds **1a–c**, **2a–c** and **3a–c**. Compounds **4a–c** were obtained by dehydrogenation of **2a–c** with 2,3-dichloro-5,6-dicyanobenzoquinone (DDQ) in dichloromethane. In

turn, esters **7–8** were prepared by dehalogenation of chloroesters **5**[10] and **6**[10] with ammonium formate in presence of 10% Pd/C in methanol. (Scheme 1). The higher homologue benzocycloheptapyrrole **9** was prepared by a sigmatropic rearrangement of the benzosuberone oxime adduct by methylpropiolate.[10, 11]
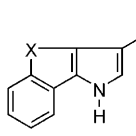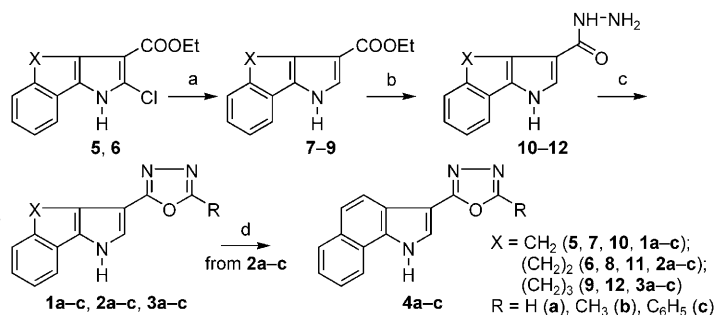

Scheme 1. Reagents and conditions: a) MeOH, HCOONH₄, Pd/C 10%; b) NH₂NH₂ H₂O 98%; c) DMF, RC(OEt)₃; d) DDQ, CH₂Cl₂.

Biological assays

Growth inhibition against a panel of 60 human cancer cell lines

The compounds were evaluated by NCI for their in vitro cytotoxic activity against 60 human tumour cell lines that are derived from nine cancer cell types. The concentrations that inhibited cell growth by 50% (GI$_{50}$, in μM) are reported in Table 1. The lead compound **A** was used as reference. Compounds **1c** and **4c** were found to be the most interesting of the series, with **4c** being generally slightly more potent than **1c**. The best activity for the latter was observed in a colon

Table 1. Growth inhibition against a panel of 60 human cancer cell lines.[a]

X = CH₂ (**1a–c**); (CH₂)₂ (**2a–c**); (CH₂)₃ (**3a–c**); CH=CH (**4a–c**)
R = H (**a**), CH₃ (**b**), C₆H₅ (**c**)

Cell Line	A	1a	1b	1c	2a	2b[c]	2c[c]	3a	3b[d]	3c	4a	4b[d]	4c
						GI$_{50}$ [μM][b]							
leukaemia	64.5	79.7	81.3	1.82	26.3	NA	NA	22.1	NT	14.1	44.6	NT	0.64
non-small cell lung cancer	100.0	57.8	93.3	3.39	21.8	NA	NA	38.2	NT	15.8	22.3	NT	2.36
colon cancer	64.5	81.2	100.0	1.00	25.7	NA	NA	30.1	NT	10.0	33.8	NT	0.70
CNS cancer	83.2	86.7	75.8	2.95	28.2	NA	NA	36.3	NT	16.2	32.3	NT	1.21
melanoma	100.0	77.3	79.4	2.34	28.8	NA	NA	42.7	NT	14.4	33.8	NT	2.71
ovarian cancer	100.0	81.2	30.2	4.57	28.2	NA	NA	44.8	NT	19.4	38.9	NT	1.70
renal cancer	100.0	67.3	91.2	6.31	27.5	NA	NA	34.9	NT	15.8	38.0	NT	2.04
prostate cancer	100.0	100.0	100.0	4.78	32.3	NA	NA	59.5	NT	16.2	62.3	NT	1.28
breast cancer	81.3	73.2	77.6	3.16	27.5	NA	NA	25.6	NT	14.7	40.2	NT	0.60
mean	85.1	74.1	75.8	2.9	26.3	NA	NA	34.6	NT	14.7	35.4	NT	1.28

[a] These data were obtained from NCI's in vitro disease-oriented tumour cell screen. [b] GI$_{50}$=drug concentration that elicits inhibition of cell growth by 50%. [c] NA=Inactive in primary anticancer assays on a cell line panel consisting of MCF7 (breast), NCI-H460 (lung), and SF-268 (CNS) cells. [d] NT=Not tested.

☜☜ These are not the final page numbers!

cancer cell line (GI$_{50}$ = 1.00 μM) whereas **4c** was particularly active against leukaemia, colon and breast cancer cell lines (GI$_{50}$ < 1.00 μM). In the same assays the reference compound **A** was less active than **1c** and **4c** in all tumour cell lines. The most interesting compounds **1c** and **4c** were selected for further evaluation to understand their possible mechanism of action. The results of the experiments discussed below are predictive of a microtubule-stabilising activity.

In vitro cell growth inhibition

The antiproliferative activity of **1c** and **4c** against a panel of human tumour cell lines, including IGROV-1 and IGROV-1/Pt1 (ovarian carcinoma cell lines), JR8 (a melanoma cell line), HT29 and HT29/MIT (colon carcinoma cell lines), was determined after 72 h of drug exposure in comparison with paclitaxel (PTX) as a reference compound. The IC$_{50}$ values are reported in Table 2. Under our experimental conditions **1c** was more potent than **4c** in the examined cell lines (ovarian and colon carcinomas and melanoma). The IGROV-1/Pt1 subline, which is characterised by a p53 mutation, was more sensitive than IGROV-1 to the antiproliferative effects of the two drugs, as is expected for antimicrotubule agents. Although **1c** and **4c**

Table 3. Percentage of cells in G1, S, and G2/M phases[a] after 24 h exposure to **1c**, **4c**, or paclitaxel (PTX) at a concentration corresponding to the IC$_{80}$ value for each cell line.[b]

Cell Line	Compound	G1	S	G2/M
IGROV-1	untreated	54.36	33.54	12.11
	1c	27.42	12.35	60.23
	4c	49.07	11.25	39.68
	PTX	5.32	5.32	94.68
IGROV-1/Pt1	untreated	36.79	30.98	32.33
	1c	20.01	2.01	77.78
	4c	38.01	10.63	51.36
	PTX	4.18	3.02	92.80
HT29	untreated	49.37	40.72	9.92
	1c	24.23	14.55	61.23
	4c	37.09	27.84	35.07
HT29/MIT	untreated	49.16	39.54	11.29
	1c	6.33	2.01	91.66
	4c	31.61	15.90	52.49
JR8	untreated	41.78	48.25	9.98
	1c	15.45	16.77	67.78
	4c	29.73	33.10	37.18

[a] Cell cycle distribution was calculated by ModFit software (Becton Dickinson). Percentages refer to the profiles shown in Figure 2. Data are the results of a single experiment carried out in duplicate. [b] The same concentrations were used for both the analysis of cell cycle distribution and that of mitosis.

Table 2. In vitro antiproliferative effect of **1c**, **4c**, and paclitaxel (PTX) on various tumour cell lines.

Cell Line	Histotype	p53	IC$_{50}$ [μM][a]		
			1c	**4c**	PTX
IGROV-1	ovarian carcinoma	wild-type	1.5 ± 0.2	3.42 ± 1.73	0.15 ± 0.03
IGROV-1/Pt1[b]	ovarian carcinoma	mut	0.63 ± 0.01	2.01 ± 1.31	0.013 ± 0.004
HT29	colon carcinoma	mut	1.30 ± 0.09	19.5 ± 1.9	0.0057 ± 0.0011
HT29/MIT[c]	colon carcinoma	mut	0.4 ± 0.1	0.8 ± 0.1	0.0045 ± 0.0021
JR8	melanoma	mut	0.39 ± 0.03	3.99 ± 1.3	–

[a] IC$_{50}$ values (± SD) represent the mean of least three independent experiments. [b] The cisplatin-resistant cell subline was selected by exposure to increasing cisplatin concentrations.[12] [c] The mitoxantrone-resistant cell subline was selected by exposure to increasing drug concentrations of up to 0.3 μg mL^{-1}.

were less potent than paclitaxel, their behaviour is typical of compounds that act by promoting tubulin polymerisation. Also in JR8, another cell line expressing a mutated p53, both drugs exhibited marked growth-inhibitory effects. As shown in Table 2, the cell lines carrying mutated p53 were sensitive to paclitaxel (IC$_{50}$ range: 0.013–0.004 μM).

Cell cycle analysis and evaluation of nuclear morphology

Because induction of mitotic arrest is a hallmark of microtubule inhibition, we examined the cell cycle perturbations of IGROV-1, IGROV-1/Pt1, HT29, HT29/MIT and JR8 cells that were exposed to **1c**, **4c** and paclitaxel at an indicative concentration of IC$_{80}$. In all of the tested cell lines after 24 h exposure at a concentration corresponding to IC$_{80}$, **1c** and **4c** induced a more marked and persistent accumulation of cells in G2/M phase than the control (Table 3 and Figure 2a). In IGROV-1 and IGROV-1/Pt1 cells this effect was more evident after paclitaxel treatment, which resulted in about 90% of cells in G2/M

phases (Table 3 and Figure 2b). A marked sub-G1 peak was already found at 24 h and increased at 48–72 h for **1c** and **4c** (Figure 2a). The analysis of morphological features of treated cells, after PI staining of nuclei, indicated a dose-dependent induction of aberrant mitosis by **1c** or **4c** treatment similar to that of paclitaxel exposure with respect to untreated cells. (Table 4)

Modulation of biochemical markers of mitotic arrest

To confirm the mitotic arrest that was observed by cell cycle and morphology analysis, we investigated the biochemical modulation of markers of M phase in IGROV-1 and in IGROV-1/Pt1 cells that were exposed to the IC$_{80}$ and IC$_{50}$ of **1c** or **4c** for 24 h. A hyperphosphorylated state of Raf-1 and Bcl-2 family members is a biochemical hallmark of the cellular response to microtubule inhibitors.[13, 14] In both cell lines drug treatment induced a parallel mobility shift of Bcl-2 and Raf-1 in SDS-PAGE, thereby indicating a drug-induced phosphorylation of the two proteins (Figure 3). Moreover, as illustrated in Figure 3, Western blot analysis detected a slower migrating band that was evidenced by the shift in the electrophoretic mobility in both of the treated cells (corresponding to phosphorylated form of cdc25C phosphatase) and an up-regulation of cyclin B1, thereby indicating an accumulation of mitosis-promoting factors. In addition, mitotic arrest was further confirmed by the increased
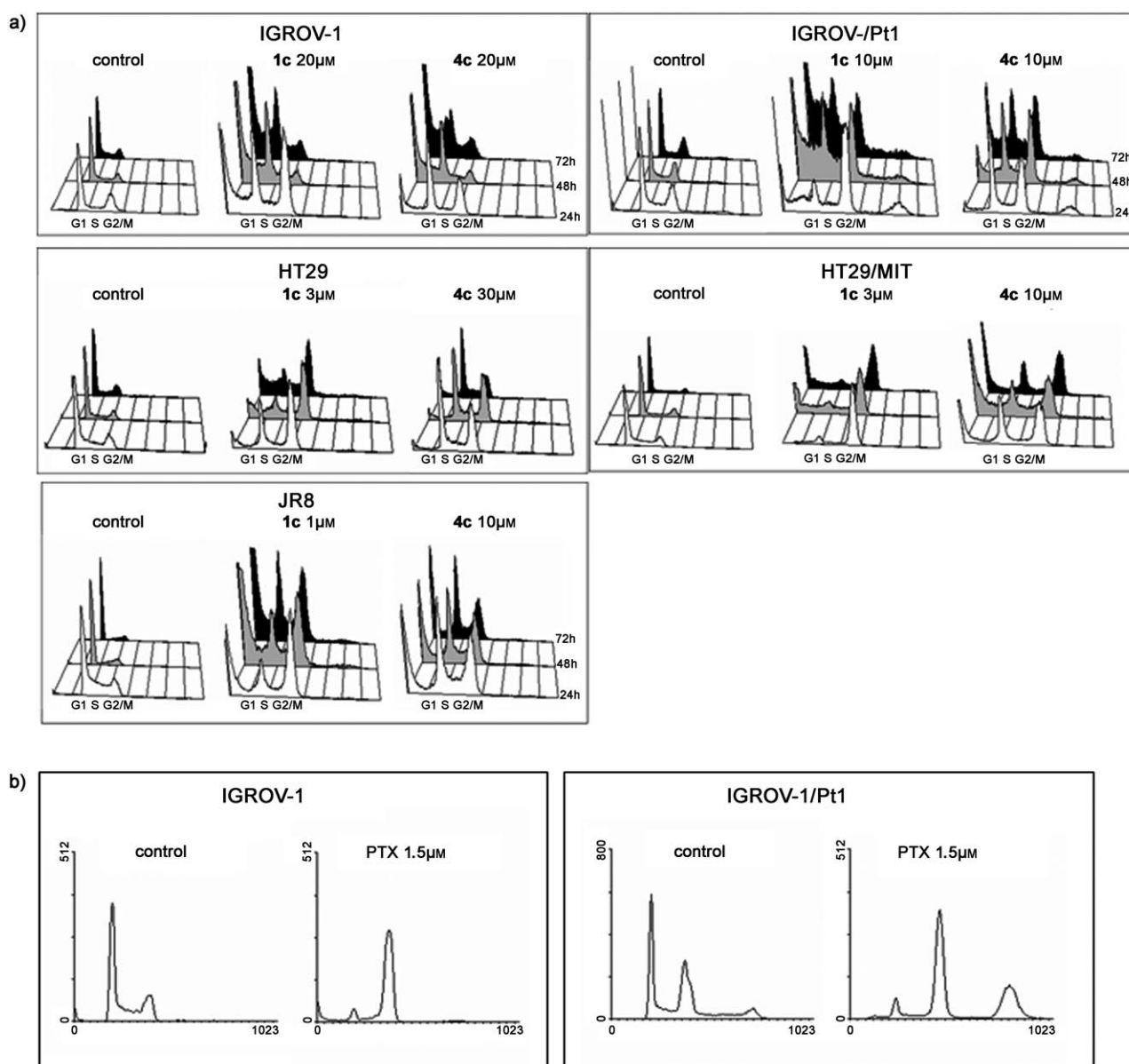
These are not the final page numbers! ➚➚

Figure 2. a) Cell cycle distribution of IGROV-1, IGROV-1/Pt1, HT29, HT29/MIT, and JR8 cells that were treated with **1 c**, **4 c** or b) paclitaxel (PTX, only for IGROV-1 and IGROV-1/Pt1 cells) at the indicated concentration (IC_{80}); profiles were obtained by flow cytometry analysis of PI-stained cells at 24, 48, or 72 h treatment as indicated. b) Cell cycle analysis of PTX-treated cells was performed 24 h after treatment. Data represent a single experiment carried out in duplicate.

reactivity of cell lysates to the MPM-2 antibody, which recognises several mitosis-specific epitopes. Because spindle damage induces up-regulation of p53 in cell lines that express the wild-type form,[15, 16] we investigated the expression level of p53 24 h after drug treatment. As shown in Figure 3, both **1 c** and **4 c** showed a marked increase of p53 expression in IGROV-1 cells.

Evaluation of microtubule organisation by immunofluorescence analysis

To investigate the drug effect on microtubule organisation as a consequence of the interaction with tubulin, we performed immunofluorescence analyses on IGROV-1, HT29 and HT29/MIT

after 24 h of treatment with a concentration corresponding to IC_{80} (Figure 4). In every cell line, β-tubulin had a widespread distribution in the cytosol of untreated cells. On the contrary, the presence of β-tubulin assembly could be detected in cells with condensed chromatin (mitotic cells) after 24 h of treatment with both **1 c** or **4 c**. Such an effect is comparable with that induced by equitoxic concentrations of paclitaxel (Figure 4). In contrast, vinorelbine caused an apparent decrease of β-tubulin expression in the cytoplasm.

Evaluation of acetylated tubulin by Western blot analysis

Because tubulin acetylation is known to reflect microtubule stabilisation during the mitotic phase of proliferating paclitax-

↖↖ These are not the final page numbers!

Table 4. Induction of mitotic cells after 24 h exposure to **1c**, **4c**, or pacli-taxel (PTX) at a concentration corresponding to the IC_{80} value for each cell line.[a]

Compound	Cell Line				
	IGROV-1	IGROV-1/Pt1	HT29	HT29/MIT	JR8
1c	30 ± 4	45 ± 12	45 ± 5	45 ± 12	40 ± 2
4c	32 ± 6	40 ± 10	27 ± 3	40 ± 10	42 ± 6
PTX	45 ± 5	55 ± 3	50 ± 4	62 ± 4	

[a] The same concentrations were used for both the analysis of cell cycle distribution and that of mitosis. The results, expressed as a percentage of the total cell population, are the mean of at least two independent experiments.
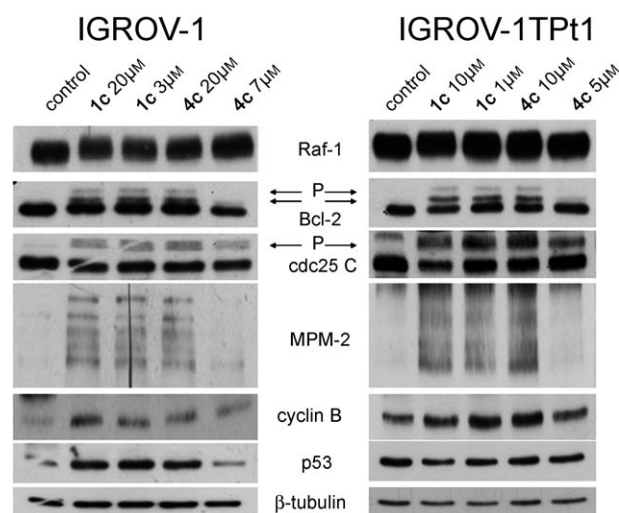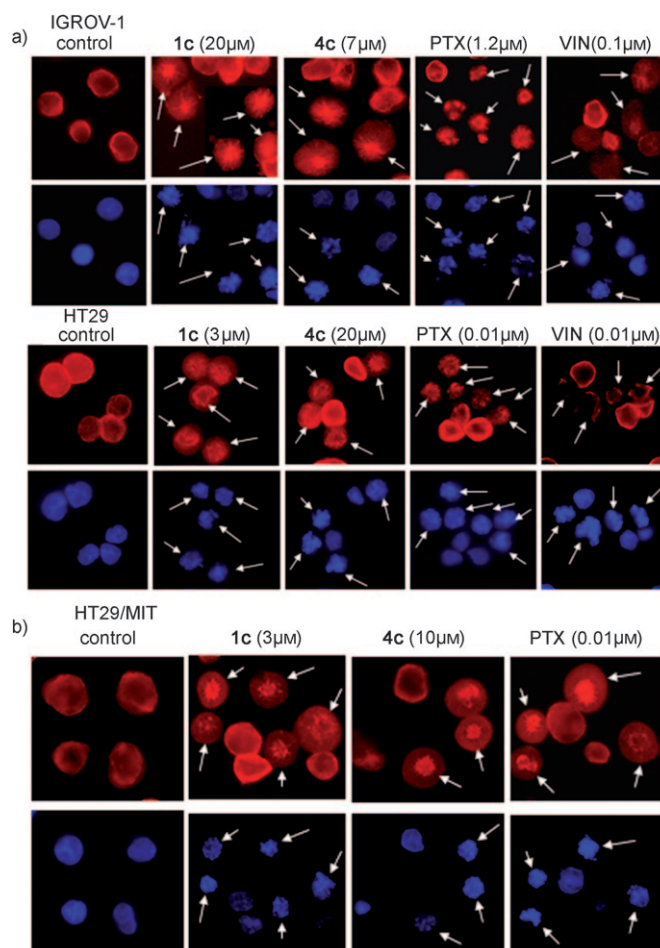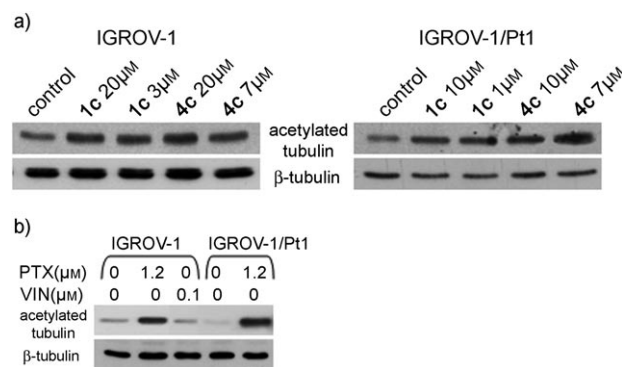

Figure 3. Biochemical effects of **1c** or **4c** (IC_{50} or IC_{80}) on IGROV-1 and IGROV-1/Pt1 cells after 24 h treatment. Modulation of p53, MPM-2 epitopes, and proteins that are involved in the G2/M phase transition was analyzed by Western blot analysis. 'P' indicates phosphorylated proteins; β-tubulin is shown as a control of protein loading.

Figure 4. Immunofluorescence staining of β-tubulin in a) IGROV-1 and HT29 and b) HT29/MIT cells. Upper panel: red β-tubulin staining; lower panel: DNA counterstained blue with Hoechst 33342. Cells were treated for 24 h with solvent, paclitaxel (PTX), vinorelbine (VIN), **1c** or **4c** at the indicated concentration corresponding to their IC_{80} values. Arrows indicate cells with β-tubulin assembly and condensed chromatin (mitotic catastrophe).

el-treated cells,[17] we analyzed the acetylation status of cells that were treated with different concentrations of **1c** and **4c** (Figure 5).

As expected, both **1c** and **4c** caused an increase of acetylat-ed tubulin in IGROV-1 and IGROV-1/Pt1 cells following 24 h exposure (Figure 5a). Accordingly, identical results were obtained with paclitaxel (Figure 5b). On the contrary, no modulation in the expression of the tubulin acetylation was observed after vinorelbine exposure (Figure 5b). The presence of β-tubulin assembly and the increase of acetylated tubulin in treated cells suggest that these compounds belong to the class of polymerising agents.

Figure 5. Effects of a) **1c** and **4c** and b) paclitaxel (PTX) and vinorelbine (VIN) on the acetylation of tubulin in IGROV-1 and IGROV-1/Pt1 cells. Cells were treated with **1c** and **4c** at both IC_{80} and IC_{50} values; paclitaxel and vi-norelbine at IC_{80}. Whole-cell extracts were prepared and analyzed by Western blot analysis. β-Tubulin is shown as a control of protein loading.

Apoptosis induction

To investigate the drugs' ability to induce apoptosis, the amount of apoptotic cells was determined by a TUNEL assay (Figure 6). Equitoxic concentrations (IC_{80}) of **1c** and **4c** produced a comparable level of apoptosis (ranging from 30% to 48%); **1c** was somewhat more effective than **4c** in IGROV-1/Pt1 cells.
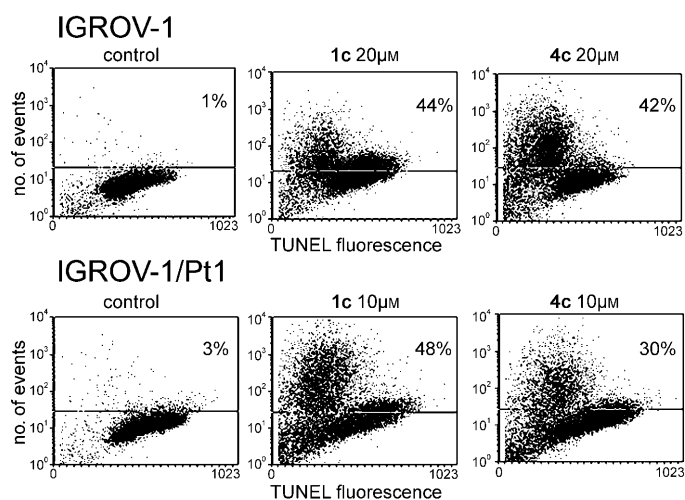
IGROV-1

IGROV-1/Pt1

Figure 6. Apoptosis in IGROV-1 and IGROV-1/Pt1 cells treated for 72 h at the IC$_{80}$ value of **1c** or **4c**. Apoptosis was assessed by FACScan analysis on TUNEL-stained cells. The percentage of TUNEL-positive cells are indicated in each panel. Results from at least two independent experiments are shown.

In vitro tubulin polymerisation

Finally, to verify that the compounds directly target tubulin, we evaluated their activity in a tubulin-assembly assay by using pure bovine tubulin. The results showed that compounds **1c** and **4c** are effective on tubulin polymerisation. The concentrations that decreased the unpolymerised fraction of tubulin by 50% are reported in Table 5; this indicates that **1c** and **4c**, although less active than paclitaxel, induce the polymerisation of tubulin at micromolar concentrations. Taken together, data from cultured cell tests and in vitro assay demonstrate that **1c** and **4c** act as antiproliferative and antimicrotubule drugs.

Table 5. Effect of **1c**, **4c**, and paclitaxel (PTX) on tubulin assembly.

Compound	EC$_{50}$ [μM][a]
PTX	3.5 ± 0.5
1c	16.4 ± 1.9
4c	9.7 ± 0.7

[a] EC$_{50}$ = drug concentration required for 50% decrease in unpolymerised tubulin following incubation for 30 min; compounds were assayed three times, and the values reported are the mean $\pm$ SEM.

Molecular modelling and docking

The studied compounds can be divided into four series (from **1** to **4**) on the basis of their structure (Figure 1): the tricyclic head can be a 1,4-dihydroindeno[1,2-*b*]pyrrole (**1a–c**), a 4,5-dihydro-1*H*-benzo[*g*]indole (**2a–c**), a 1,4,5,6-tetrahydro-benzo-[6,7]cyclohepta[1,2-*b*]pyrrole (**3a–c**), or an 1*H*-benzo[*g*]indole (**4a–c**). Each series can be further split into three sub-series (a, b and c), depending on the nature of the side chain on the oxadiazole ring. The conformational analysis shows that each of the analysed compounds can exist in two conformations that

differ for the orientation of the oxadiazole ring with respect to the pyrrole ring and present only a small energy difference (usually lower than 2 kcal mol^{-1}). The only exception is represented by the 1,4,5,6-tetrahydro-benzo[6,7]cyclohepta[1,2-*b*]pyrrole derivatives (**3a–c**), which contain a more flexible seven-membered ring and present four different conformations that are derived from the two possible puckered conformations of the seven-membered ring. Compounds belonging to the **1** and **4** series are completely planar molecules, whereas the series **2** and **3** deviate from planarity by 11° and 25°, respectively (see τ_1 values in Table 6).

Table 6. Torsion angles (τ [°]) of the studied oxadiazole systems obtained through conformational analysis (CA) and molecular docking.

Compd	GI$_{50}$	CA		Site 1		Site 2	
		τ_1	τ_2	τ_1	τ_2	τ_1	τ_2
1a	74.1	0	180.0	0	−67.6	0	−101.0
1b	75.8	0	180.0	0	103.9	0	112.1
1c	2.90	0	180.0	0	105.3	0	65.8
2a	26.6	11.4	−178.7	−8.9	−77.4	−8.9	116.1
2b	NA	11.4	−178.7	−8.9	−71.8	−8.9	124.5
2c	NA	11.4	−178.7	−8.8	−75.5	−8.8	97.3
3a	34.6	−25.3	−178.5	2.8	100.7	2.8	123.4
3b	NT	−25.3	−178.5	−2.9	−85.5	−2.9	124.2
3c	14.7	−25.4	0.6	−3.1	−84.0	−3.1	126.5
4a	35.4	0	180.0	0	−68.8	0	112.6
4b	NT	0	180.0	0	−74.2	0	120.2
4c	1.28	0	180.0	0	−78.3	0	−104.6

Therefore, because both geometrical and electronic features, such as planarity, HOMO–LUMO energy, nitrogen–nitrogen and nitrogen–oxygen atom distances do not seem to be easily associable with activity, the first step that we characterised in detail was the binding site of the oxadiazole derivatives. Crystallographic data that was retrieved from the Protein Data Bank (entry 1SA1[7]) contain a dimer of α- and β-tubulin in complex with podophyllotoxin. The docking process was performed in two steps by using the docking program Auto-Dock.[18–21] In the first step, a procedure resembling the so-called "blind docking" approach was used to obtain an approximate binding mode between the two most active ligand (**1c** and **4c**) and tubulin.[22,23] The resulting conformations were clustered and most of them (up to 67% of the docking solutions) were found to be located at the interface between the α- and β-tubulin subunits. The most important residues (within 5 Å of the ligand) form this binding site (site 1) and correspond mainly to Gln176, Ser178 and Thr179 (α-subunit), Gln247, Leu248, Asp329, Leu333, Lys352, and Thr353 (β-subunit). Up to 30% of the remaining docking solutions were found within the α-tubulin subunit (site 2), which is constituted by Gln11, Asp69, Ala99, Ala100, Asn101, Gly143, Gly144, Thr145, Ile171, Pro173, Ala174, Ser178, Asn206, and Tyr224.

The comparison between the podophyllotoxin binding site and site 1 reveals a different amino acidic composition. For podophyllotoxin (and partially for colchicine), the pharmacophore model that was obtained by analysing its interaction with tubulin, the binding site is surrounded by Val238, Cys241, Leu242, Ala250, Leu255, Met259, Ala316, Val318, Lys352, and Ile378, which all belong to the tubulin β-subunit. In the case of site 1, it is delimited by Gln176, Ser178 and Thr179 (α-subunit), Gln247, Leu248, Asp329, Leu333, Lys352, and Thr353 (β-subunit). The only residue that is shared between the two binding sites is Lys352, a residue that makes hydrophobic contacts only through its carbon chain in the podophyllotoxin model, but in our interaction model this residue is important (together with Thr353) in the modulation of the binding affinity. The approximate location of these binding sites was then used as the starting point for the second "refined docking" run. The oxadiazole derivatives were docked in each of the putative sites and the complexes were again minimised. The first binding-site region (site 1) is characterised by the formation of at least two hydrogen bonds between the oxadiazole nitrogen atoms and NThr353 of the β-tubulin subunit, whereas in site 2, the studied ligands link mainly to OTyr224 and OThr179 of α-tubulin, with different hydrogen bonds. The main difference between the two binding sites is represented by the capacity of site 1 to accommodate all the oxadiazole derivatives (Figure 7).

This result is confirmed by the values of the calculated free energy; these values are favourable to site 2 only for compounds **1 b**, **3 b** and **2**–**4 a**, which have the oxadiazole ring either unsubstituted or substituted by a methyl group. For these reasons, the subsequent analysis of the docking results was concentrated on the first binding site (site 1). The oxadiazole substituents pointed toward a hydrophobic region that is located near the opening of the cavity and constituted principally by the lateral chains of Leu333 (see Figure 8). Although this protein region is characterised by the absence of hydrogen bond interactions, the presence of the phenyl ring seems to have a great impact on the activity (Table 1), probably due to the optimal occupancy of the binding site by the aromatic moieties (compounds **1**–**4 c**).

In this orientation, the oxadiazole ring of both **1 c** and **4 c** (the most-active derivatives in the series) is located in the middle of the binding region with the two heterocyclic nitrogen atoms oriented toward NThr353 and $O^{\gamma 1}$Thr353; this gives
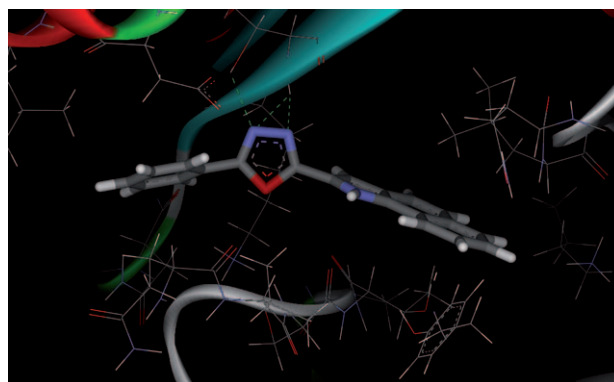

Figure 8. Detail of the three hydrogen bonds (greed dashed lines) located between the bioactive orientation of **4 c** (rendered in stick and coloured by atom type) and $O^{\gamma 1}$Thr353 and NThr353.

rise to the formation of three hydrogen bonds (two with NThr353 and one with $O^{\gamma 1}$Thr353) that allow for the stabilisation of the complex. The importance of these hydrogen bond interactions for the tubulin binding is supported by considering that the three hydrogen bonds are retained in nearly all of the compounds studied (except for **1 a**, **2 a**, and **3 b**).

The tricyclic moiety of all the studied compounds is located inside a narrow hydrophobic region that is delimited mainly by the side chains of the residues Thr198, Leu248, Ala256, Val260, Pro261, Phe262, and Pro263 (from β-tubulin subunit). The orientation of the tricyclic moiety is almost the same for all the ligands, with the exceptions of **1 b**, **1 c** and **3 a**, which are located in the same hydrophobic region but with a different orientation of their tricyclic moiety. The comparison of the torsion angle values τ_1 of the best conformations in water with those resulting from the molecular docking runs shows that for both sites the compounds are placed in the binding site in a conformation that permits hydrogen bonding without a severe modification of the planarity of the A–C ring system (Table 6). The same is not true for the τ_2 torsion angle, with some meaningful differences between the best conformations in water and those that were obtained by docking. It is important to note how the different tricyclic ring structure is implicated in the binding affinity variations, because of the presence of a number of bad contacts, mainly with the side chain of Lys352 and Thr353. In this respect, the **4 c** and **1 c** tricyclic moiety can interact with this narrow hydrophobic region by assuming an efficient planar conformation and by decreasing the number of bad contacts with the residue side chains.

A similar conformation cannot be assumed by **2 a**–**c** and **3 a**–**c** derivatives, and the resulting "bad" interactions could be responsible for the highest GI_{50} values observed; this assumption was also confirmed by the analysis of the correlation coeffi-
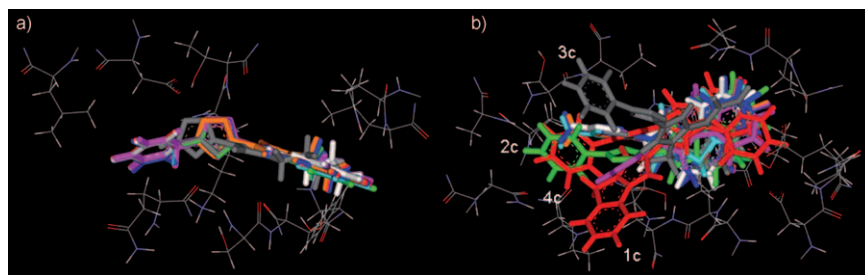

Figure 7. Superposition of the ligands docked into a) site 1 and b) site 2. In binding site 1, all of the ligands are oriented similarly (with the exception of **3 a**, in grey), whereas for site 2, varying orientations for **1 c**, **2 c**, **3 c**, and **4 c** were observed with respect to the other ligands.

These are not the final page numbers! ↗↗

cients that were obtained between the calculated docking energies and the GI_{50} values (Table 7). Indeed, the correlation coefficients that were calculated between GI_{50} and the interaction and van der Waals energy values support the importance of the steric effects in the oxadiazole derivatives' binding to tubulin. The van der Waals energy descriptor is the most statistically significant element for the quality assessment of this binding model, with a correlation coefficient up to -0.90 for site 1; these results point out that the proposed binding model would be able to explain the biological data for all compounds on the basis of their docking energies.

Table 7. Calculated values for the number of torsions, interaction energy (E) and van der Waals energy (E_{vdW}) of the oxadiazole derivatives in their docked conformations to both sites 1 and 2.

Compound	GI_{50}[a]	No. Torsion	Site 1		Site 2	
			E_i [kcal mol^{-1}]	E_{vdW} [kcal mol^{-1}]	E_i [kcal mol^{-1}]	E_{vdW} [kcal mol^{-1}]
1a	74.1	1	-100.98	23.71	-94.52	23.95
1b	75.8	1	-122.14	23.53	-98.34	23.49
1c	2.90	2	-137.90	50.61	-124.45	47.93
2a	26.6	1	-123.36	38.38	-98.61	38.41
2b	NA	1	-130.92	38.15	-104.77	38.16
2c	NA	2	-146.01	62.56	-131.11	62.63
3a	34.6	1	-119.09	31.70	-99.06	31.55
3b	NT	1	-133.46	31.41	-108.18	31.27
3c	14.7	2	-129.80	56.28	-134.29	55.55
4a	35.4	1	-123.70	44.76	-99.53	44.94
4b	NT	1	-131.127	44.50	-105.07	44.53
4c	1.28	2	-137.52	68.90	-131.62	68.73
	correlation coefficients:		0.84	-0.90	0.78	-0.88

[a] NA = Inactive; NT = Not tested.

Conclusions

We have identified a novel series of antimicrotubule agents that are characterised by a tricyclic system with 1,3,4-oxadiazol-2-yl-pyrrole moiety. The cytotoxic activity of several new compounds was better than that of the lead compound **A** (**A**: $GI_{50} = 85.1$ μM, **1c**: $GI_{50} = 2.9$ μM, **4c**: $GI_{50} = 1.28$ μM). We also demonstrated with a series of experiments (analysis of cell cycle, tubulin polymerisation, modulation of mitotic markers of M phase and apoptosis) that the antimitotic activity is the primary mechanism of their cytotoxic effects. The experiment that were performed on isolated tubulin confirm that compounds **1c** and **4c** exhibited a mechanism of action that is similar to that of taxanes, which promote tubulin polymerisation. The proposed mechanism of action was consistent with molecular modelling and docking studies. According to modelling studies, the potency is probably related to the planarity of the condensed system. In particular, series **2a–c** and **3a–c**, which lack planarity are either poorly active or inactive. These findings have encouraged us to explore novel analogues with various substituents to improve their solubility and investigate their in vivo efficacy as antitumour agents.

Experimental Section

General procedures

Unless otherwise noted, all materials were obtained from commercial suppliers and used without purification. Flash chromatography was performed by using Merck Silica gel 60 (230–400 mesh ASTM). Thin-layer chromatography (TLC) was performed with Polygram® SIL N-HR-/HV254 pre-coated plastic sheet (0.2 mm). ^{1}H and ^{13}C NMR spectra were determined in CDCl$_3$ with a superconducting FT-NMR by using a XL-200 Varian apparatus at 200 MHz. Chemical shifts are expressed in δ (ppm) downfield from internal TMS and coupling constants are expressed in Hz. ^{1}H NMR spectroscopic data

are reported in the following order: multiplicity (s, singlet; br s, broad singlet; d, doublet; dd, doublet of doublets; t, triplet; q, quartet; m, multiplet), coupling constants in Hz, number of protons, and the assignment. IR spectra were recorded as thin films or Nujol mulls on NaCl plates with a PerkinElmer 781 IR spectrophotometer and are expressed in $\tilde{\nu}$ (cm^{-1}). Melting points were determined on a Thomas Hoover capillary melting point apparatus and are uncorrected. All compounds were crystallised from EtOH. Elemental analyses are within ±0.4% of the theoretical values. Starting products **5**, **6** and **9** were prepared as previously described.[10]

General procedure I: *Synthesis of tricyclic esters* **7** *and* **8**. 10% Pd/C (0.18 g) was added to a solution of chloro ester (**5**, **6**; 2.72 mmol) and HCOONH$_4$ (13.6 mmol) in MeOH (22 mL). The mixture was stirred under N$_2$ for 3–4 h, then filtered through Celite, and the solution was evaporated under vacuum. The residue was purified by flash chromatography by eluting with petroleum ether (PE)/EtOAc (8:2) to give the desired products **7**, **8**.

Ethyl 1,4-dihydro-indeno[1,2-*b*]pyrrole-3-carboxylate (**7**). General procedure I was used to convert **5** into the title compound **7**. Yield: 77%; $R_f = 0.32$ (PE/EtOAc, 8:2); mp: 176–178 °C; ^{1}H NMR [300 MHz CDCl$_3$]: δ = 1.39 (t, 3H, CH$_3$), 3.70 (s, 2H, CH$_2$), 4.35 (q, 2H, CH$_2$), 7.14 (d, 1H, CH), 7.23 (s, 1H, CH), 7.32 (t, 1H, CH), 7.48 (s, 1H, CH), 7.51 (d, 1H, CH), 8.82 ppm (br s, 1H, NH exchanged with D$_2$O); IR (KBr): $\tilde{\nu}$ = 1670 (C=O), 3240 cm^{-1} (NH).

Ethyl 4,5-dihydro-1*H*-benzo[*g*]indole-3-carboxylate (**8**). General procedure I was used to convert **5** into the title compound **8**. Yield: 72%; $R_f = 0.26$ (PE/EtOAc, 8:2); mp: 140–142 °C; ^{1}H NMR [300 MHz CDCl$_3$]: δ = 1.36 (t, 3H, CH$_3$), 2.98 (t, 2H, CH$_2$), 3.04 (t, 2H, CH$_2$), 4.32 (q, 2H, CH$_2$), 7.14–7.25 (m, 4H, CH), 7.43 (d, 1H, CH), 8.65 ppm (br s, 1H, NH exchanged with D$_2$O); IR (KBr): $\tilde{\nu}$ = 1660 (C=O), 3250 cm^{-1} (NH).

General procedure II: *Synthesis of carbohydrazides* **10**, **11**, *and* **12**. A mixture of ester **7**, **8**, **9** (2 mmol), and hydrazine hydrate (1.94 mL, 40 mmol) was held at reflux for 0.5 h and then poured onto ice. The solid precipitate was filtered and washed with H$_2$O to give a crude product that was purified by trituration with EtOH.

1,4-Dihydro-indeno[1,2-*b*]pyrrole-3-carbohydrazide (**10**). General procedure II was used to convert **7** and hydrazine hydrate 98% in H$_2$O into the title compound **10**. Yield: 80%; $R_f = 0.46$ (CHCl$_3$/

CH$_3$OH, 9:1); mp: 254–256 °C; ^{1}H NMR [300 MHz CDCl$_3$ + DMSO]: δ = 3.65 (s, 2H, CH$_2$), 7.06 (t, 1H, CH), 7.42 (d, 2H, 2×CH), 7.88 (s, 1H, CH), 8.68 (br s, 1H, NH exchanged with D$_2$O), 11.44 ppm (br s, 1H, NH exchanged with D$_2$O); IR (KBr): $\tilde{v}$ = 1650 (C=O), 3190–3270 cm^{-1} (NH$_2$).

4,5-Dihydro-1*H*-benzo[*g*]indole-3-carbohydrazide (**11**). General procedure II was used to convert **8** and hydrazine hydrate 98% in H$_2$O into the title compound **11**. Yield: 80%; R_f = 0.71 (CHCl$_3$/CH$_3$OH, 9:1); mp: 268–270 °C; ^{1}H NMR [300 MHz CDCl$_3$ + DMSO]: δ = 2.66 (t, 2H, CH$_2$), 2.84 (t, 2H, CH$_2$), 4.30 (br s, 1H, NH$_2$ exchanged with D$_2$O), 6.66 (s, 1H, CH), 7.08 (d, 1H, CH), 7.17 (t, 2H, 2×CH), 7.80 (d, 1H, CH), 9.25 (br s, 1H, NH exchanged with D$_2$O), 11.68 ppm (br s, 1H, NH exchanged with D$_2$O); IR (KBr): $\tilde{v}$ = 1655 (C=O), 3140–3240 (NH$_2$), 3300 cm^{-1} (NH).

4,5-Dihydro-1*H*-benzo[*g*]indole-3-carbohydrazide (**12**). General procedure II was used to convert **9** and hydrazine hydrate 98% in H$_2$O into the title compound **12**. Yield: 82%; R_f = 0.81 (CHCl$_3$/CH$_3$OH, 9:1); mp: 302–304 °C; ^{1}H NMR [300 MHz CDCl$_3$ + DMSO]: δ = 1.97–2.05 (m, 2H, CH$_2$), 2.70–2.83 (m, 4H, 2×CH$_2$), 6.72 (s, 1H, CH), 7.12–7.27 (m, 3H, 3×CH), 7.64 (d, 1H, CH), 9.30 (br s, 1H, NH exchanged with D$_2$O), 10.66 (br s, 1H, NH exchanged with D$_2$O); IR (KBr): $\tilde{v}$ = 1625 (C=O), 3320–3360 (NH$_2$), 3350 cm^{-1} (NH).

General procedure III: *Synthesis of 1,3,4-oxadiazoles 1 a–c, 2 a–c, and 3 a–c.* A mixture of hydrazide **10**, **11**, **12** (2.5 mmol) and appropriate orthoesters (2.7 mmol) was held at reflux for 8 h and then poured onto ice. The solid precipitate was filtered and washed with H$_2$O to give a crude product that was purified by trituration with EtOH.

3-[1,3,4-Oxadiazol-2-yl]-1,4-dihydroindeno[1,2-*b*]pyrrole (**1 a**). General procedure III was used to convert **10** and ethyl orthoformate into the title compound **1 a**. Yield: 75%; R_f = 0.54 (CHCl$_3$/CH$_3$OH, 9:1); mp: 275–278 °C; ^{1}H NMR [300 MHz DMSO]: δ = 3.68 (s, 2H, CH$_2$), 7.14 (t, 1H, CH), 7.31 (t, 1H, CH), 7.51 (d, 1H, CH), 7.54 (d, 1H, CH), 7.68 (s, 1H, CH), 9.16 (s, 1H, CH), 12.12 (br s, 1H, NH exchanged with D$_2$O); IR (KBr): $\tilde{v}$ = 1605 (C=N), 3180 cm^{-1} (NH); Anal. calcd (%) for C$_{13}$H$_9$N$_3$O: C 69.94, H 4.06, N 18.82, found: C 70.24, H 4.46, N 19.00.

3-[1,3,4-Oxadiazol-5-methyl-2-yl]-1,4-dihydroindeno[1,2-*b*]pyrrole (**1 b**). General procedure III was used to convert **10** and ethyl orthoacetate into the title compound **1 b**. Yield: 82%; R_f = 0.81 (CHCl$_3$/CH$_3$OH, 9:1); mp: 302–304 °C; ^{1}H NMR [300 MHz DMSO]: δ = 2.55 (s, 3H, CH$_3$), 3.67 (s, 2H, CH$_2$), 7.10 (t, 1H, CH), 7.26 (t, 1H, CH), 7.45–7.50 (d, 3H, 3×CH), 11.83 (br s, 1H, NH exchanged with D$_2$O); IR (KBr): $\tilde{v}$ = 1620 cm^{-1} (C=N); Anal. calcd (%) for C$_{14}$H$_{11}$N$_3$O: C 70.87, H 4.67, N 17.71, found: C 70.48, H 4.29, N 17.53.

3-[1,3,4-Oxadiazol-5-phenyl-2-yl]-1,4-dihydroindeno[1,2-*b*]pyrrole (**1 c**). General procedure III was used to convert **10** and ethyl orthobenzoate into the title compound **1 c**. Yield: 82%; R_f = 0.83 (CHCl$_3$/CH$_3$OH, 9:1); mp: 350 °C (dec); ^{1}H NMR [300 MHz CF$_3$COOD]: δ = 3.82 (s, 2H, CH$_2$), 7.20–7.40 (m, 2H, 2×CH), 7.52 (t, 2H, 2×CH), 7.68–7.96 (m, 4H, 4×CH), 8.16–8.20 (d, 2H, CH$_2$), 11.60 (br s, 1H, NH exchanged with D$_2$O); IR (KBr): $\tilde{v}$ = 1610 cm^{-1} (C=N); Anal. calcd (%) for C$_{19}$H$_{13}$N$_3$O: C 76.24, H 4.37, N 14.03, found: C 76.44, H 4.42, N 14.19.

3-[1,3,4-Oxadiazol-2-yl]-4,5-dihydro-1*H*-benzo[*g*]indole (**2 a**). General procedure III was used to convert **11** and ethylorthoformate into the title compound **2 a**. Yield: 93%; R_f = 0.65 (CHCl$_3$/CH$_3$OH, 9:1); mp: 198–200 °C; ^{1}H NMR [300 MHz CDCl$_3$ + DMSO]: δ = 2.84 (t, 2H, CH$_2$), 2.91 (t, 2H, CH$_2$), 7.26–7.38 (m, 3H, 3×CH), 7.45 (s, 1H, CH), 7.57 (d, 1H, CH), 8.56 (d, 1H, CH), 11.12 (br s, 1H, NH ex-

changed with D$_2$O); IR (KBr): $\tilde{v}$ = 1600 (C=N), 3170 cm^{-1} (NH); Anal. calcd (%) for C$_{14}$H$_{11}$N$_3$O: C 70.87, H 4.67, N 17.71, found: C 70.52, H 4.31, N 17.52.

3-[1,3,4-Oxadiazol-5-methyl-2-yl]-4,5-dihydro-1*H*-benzo[*g*]indole (**2 b**). General procedure III was used to convert **10** and ethyl orthoacetate into the title compound **2 b**. Yield: 96%; R_f = 0.67 (CHCl$_3$/CH$_3$OH, 9:1); mp: 201–203 °C; ^{1}H NMR [300 MHz CDCl$_3$ + DMSO]: δ = 2.57 (s, 3H, CH$_3$), 2.96 (t, 2H, CH$_2$), 3.05 (t, 2H, CH$_2$), 7.08–7.24 (m, 3H, 3×CH), 7.35–7.45 (m, 2H, 2×CH), 10.95 (br s, 1H, NH exchanged with D$_2$O); IR (KBr): $\tilde{v}$ = 1620 (C=N), 3250 cm^{-1} (NH) Anal. calcd (%) for C$_{15}$H$_{13}$N$_3$O: C 71.69, H 5.21, N 16.72, found: C 72.01, H 5.28, N 16.97.

3-[1,3,4-Oxadiazol-5-phenyl-2-yl]-4,5-dihydro-1*H*-benzo[*g*]indole (**2 c**). General procedure III was used to convert **10** and ethyl orthobenzoate into the title compound **2 c**. Yield: 95%; R_f = 0.77 (CHCl$_3$/CH$_3$OH, 9:1); mp: 297–298 °C; ^{1}H NMR [300 MHz CDCl$_3$ + DMSO]: δ = 3.01 (t, 2H, CH$_2$), 3.13 (t, 2H, CH$_2$), 7.09–7.25 (m, 3H, 3×CH), 7.49–7.57 (m, 5H, 5×CH), 8.06–8.11 (m, 2H, 2×CH), 11.65 (br s, 1H, NH exchanged with D$_2$O); IR (KBr): $\tilde{v}$ = 1640 (C=N), 3170 cm^{-1} (NH) Anal. calcd (%) for C$_{20}$H$_{15}$N$_3$O: C 76.66, H 4.82, N 13.41, found: C 76.85, H 5.20, N 13.54.

3-[1,3,4-Oxadiazol-2-yl]-1,4,5,6-tetrahydrobenzo[6,7]cyclohepta-[1,2-*b*]pyrrole (**3 a**). General procedure III was used to convert **10** and ethylorthoformate into the title compound **3 a**. Yield: 86%; R_f = 0.89 (CHCl$_3$/CH$_3$OH, 9:1); mp: 238–240 °C; ^{1}H NMR [300 MHz CDCl$_3$ + DMSO]: δ = 2.23–2.33 (t, 2H, CH$_2$), 2.57–2.64 (t, 2H, CH$_2$), 2.79–2.86 (m, 2H, CH$_2$), 7.16–7.45 (m, 5H, 5×CH), 8.28 (s, 1H, CH), 9.99 (br s, 1H, NH exchanged with D$_2$O); IR (KBr): $\tilde{v}$ = 1630 cm^{-1} (C=N); Anal. calcd (%) for C$_{15}$H$_{13}$N$_3$O: C 71.69, H 5.21, N 16.72, found: C 72.00, H 5.58, N 16.88.

3-[1,3,4-Oxadiazol-5-metyl-2-yl]-1,4,5,6-tetrahydrobenzo-[6,7]cyclohepta[1,2-*b*]pyrrole (**3 b**). General procedure III was used to convert **10** and ethyl orthoacetate into the title compound **3 b**. Yield: 45%; R_f = 0.94 (CHCl$_3$/CH$_3$OH, 9:1); mp: 195–198 °C; ^{1}H NMR [300 MHz CDCl$_3$ + DMSO]: δ = 1.99–2.18 (m, 2H, CH$_2$), 2.57 (s, 3H CH$_3$), 2.79–2.90 (m, 4H, 2×CH$_2$), 7.17–7.30 (m, 4H, 4×CH), 7.52 (d, 1H, CH), 9.56 (br s, 1H, NH exchanged with D$_2$O); IR (KBr): $\tilde{v}$ = 1625 cm^{-1} (C=N); Anal. calcd (%) for C$_{16}$H$_{15}$N$_3$O: C 72.43, H 5.69, N 15.84, found: C 72.05, H 5.32, N 15.67.

3-[1,3,4-Oxadiazol-5-phenyl-2-yl]-1,4,5,6-tetrahydrobenzo-[6,7]cyclohepta[1,2-*b*]pyrrole (**3 c**). General procedure III was used to convert **10** and ethyl orthobenzoate into the title compound **3 c**. Yield: 50%; R_f = 0.72 (CHCl$_3$/CH$_3$OH, 9:1); mp: 170–172 °C; ^{1}H NMR [300 MHz CDCl$_3$ + DMSO]: δ = 1.98–2.15 (m, 2H, CH$_2$), 2.80–2.92 (m, 4H, 2×CH$_2$), 6.87 (s, 1H CH), 7.15–7.25 (m, 4H, 4×CH), 7.38–7.58 (m, 3H, 3×CH), 7.63–7.73 (m, 2H, 2×CH), 9.48 (br s, 1H, NH exchanged with D$_2$O); IR (KBr): $\tilde{v}$ = 1620 cm^{-1} (C=N), 3175 (NH); Anal. calcd (%) for C$_{21}$H$_{17}$N$_3$O: C 77.04, H 5.23, N 12.83, found: C 77.88, H 4.90, N 12.70.

General procedure IV: *Synthesis of 1,3,4-oxadiazoles 4 a–c.* DDQ (7.98 mmol) was added to a solution of **2 a–c** (2.66 mmol) in CH$_2$Cl$_2$ (10 mL). The mixture was stirred for 5 min. The solvent was evaporated, and the residue was purified by flash chromatography by eluting with CH$_2$Cl$_2$/MeOH (8:2).

3-[1,3,4-Oxadiazol-2-yl]-1*H*-benzo[*g*]indole (**4 a**). General procedure IV was used to convert **2 a** into the title compound **4 a**. Yield: 64%; R_f = 0.65 (CHCl$_3$/CH$_3$OH, 9:1); mp: 277–278 °C; ^{1}H NMR [300 MHz CDCl$_3$ + DMSO]: δ = 7.41–7.55 (m, 3H, 3×CH), 7.62 (d, 1H, CH), 7.88 (d, J = 6.4 Hz, 1H, CH), 8.23 (d, 1H, CH), 8.30 (d, J = 6.4 Hz, 1H, CH), 8.34 (d, 1H, CH), 12.10 (br s, 1H, NH exchanged

These are not the final page numbers! ↗↗

with D$_2$O); IR (KBr): $\tilde{v} = 1615$ (C=N), 3180 cm^{-1} (NH); Anal. calcd (%) for C$_{14}$H$_9$N$_3$O: C 71.48, H 3.85, N 17.86, found: C 71.34, H 4.23, N 18.03.

3-[1,3,4-Oxadiazol-5-methyl-2-yl]-1H-benzo[g]indole (**4b**). General procedure IV was used to convert **2b** into the title compound **4b**. Yield: 91%; $R_f = 0.67$ (CHCl$_3$/CH$_3$OH, 9:1); mp: 326–328 °C; ^{1}H NMR [300 MHz CDCl$_3$ + DMSO]: $\delta = 2.64$ (s, 3 H, CH$_3$), 7.44 (s, 1 H, CH), 7.45–7.61 (m, 2 H, 2×CH), 7.67 (d, 1 H, CH $J = 8.8$ Hz), 7.93 (d, 1 H, CH), 8.32 (d, $J = 8.8$ Hz, 1 H, CH), 8.38 (d, 1 H, CH), 12.03 (br s, 1 H, NH exchanged with D$_2$O); IR (KBr): $\tilde{v} = 1620$ cm^{-1} (C=N); Anal. calcd (%) for C$_{15}$H$_{11}$N$_3$O: C 72.27, H 4.45, N 16.85, found: C 71.94, H 4.06, N 16.68.

3-[1,3,4-Oxadiazol-5-phenyl-2-yl]-1H-benzo[g]indole (**4c**). General procedure IV was used to convert **2c** into the title compound **4c**. Yield: 38%; $R_f = 0.77$ (CHCl$_3$/CH$_3$OH, 9:1); mp: 328–329 °C; ^{1}H NMR [300 MHz CDCl$_3$ + DMSO]: $\delta = 7.48$–7.61 (m, 5 H, 5×CH), 7.62 (s, 1 H, CH), 7.68 (d, $J = 8.8$ Hz, 1 H, CH), 7.96 (d, 1 H, CH), 8.11 (d, 1 H, CH), 8.15 (d, 1 H, CH), 8.26 (d, $J = 8.8$ Hz, 1 H, CH), 8.44 (d, 1 H, CH), 13.42 (br s, 1 H, NH exchanged with D$_2$O); IR (KBr): $\tilde{v} = 1630$ (C=N), 3160 cm^{-1} (NH); Anal. calcd (%) for C$_{20}$H$_{13}$N$_3$O: C 77.15, H 4.20, N 13.49, found: C 77.54, H 4.52, N 13.62.

Antibodies

Anti-cyclin B1, anti-cdc25C, and anti-Raf-1 were purchased from Santa Cruz Biotechnology (Santa Cruz, CA, USA). The mitotic protein monoclonal-2 (MPM-2) was from Upstate Biotechnology (Lake Placid, NY, USA). The monoclonal antibody against p53 or Bcl-2 was from Dako (Glostrup, Denmark). A mouse anti-β tubulin and a mouse anti-acetylated tubulin antibody were from Sigma (St. Louis, MO, USA).

Cell lines and cellular sensitivity studies

The human ovarian carcinoma cell line IGROV-1 and the cisplatin-resistant subline IGROV-1/Pt1, which was selected by exposure to increasing drug concentrations,[12] were maintained in RPMI-1640 (Lonza, Verviers, Belgium) supplemented with 10% foetal calf serum (FCS; Life Technologies, Inc., Gaithersburg, MD, USA). Cells from the human melanoma cell line JR8 were maintained in the same conditions. The colon cancer cell line HT29 and the mitoxantrone-resistant subline HT29/MIT, which was selected for resistance to mitoxantrone and overexpressing BCRP[24] were maintained in McCoy's 5A medium (Lonza) that was supplemented with 10% FCS (Life Technologies). Cellular sensitivity to drugs was assessed by a growth–inhibition assay. Cells in the logarithmic phase of growth were seeded in duplicates into 12-well plates and, 24 h later, exposed to drug for 72 h. Cells were counted by a Coulter counter (Coulter Electronics, Luton, UK) and the IC$_{50}$ values were calculated from the dose–response curves and were defined as drug concentration required for 50% growth inhibition of treated cells over untreated control.

Cell cycle analysis and the evaluation of nuclear morphology

Following drug exposure for 24 h, floating and adherent cells were collected and fixed in 70% ice-cold EtOH. Thereafter, samples were incubated with a solution of propidium iodide (PI, 10 μg mL^{-1}; Sigma) and RNAse (66 U mL^{-1}; Sigma) in phosphate-buffered saline (PBS). Cell cycle distribution was analysed on at least 40 000 cells by a FACScan flow cytometer that was equipped with an argon laser (Becton Dickinson, Mountain View, CA, USA) and then quantified by ModFit software. Cells with a mitotic morphology (i.e., characterised by a regular distribution of intense chromatin regions) were counted by fluorescence microscopy. At least 200 cells in two different smears were examined.

Western blot analysis

Cells were exposed to the drug at the indicated concentrations for 24 h. Floating and adherent cells, were collected, and whole-cell extracts were prepared as previously described.[25] Equal amounts of proteins were fractionated by SDS-PAGE and transferred onto nitrocellulose membranes. The filters were incubated with primary antibodies and then with anti-mouse or anti-rabbit horseradish-peroxidase-conjugated secondary antibodies. Immunoreactive bands were visualised by the Amersham chemiluminescence system (Amersham, Little Chalfont, UK).

Immunofluorescence staining of β-tubulin

IGROV-1, HT29 and HT29/MIT were exposed to the drug (IC$_{80}$) for 24 h. At the end of treatment, cells were fixed in 4% paraformaldehyde in PBS for 30 min, washed in PBS and permeabilised in 100% MeOH at −20 °C for 20 min. Cells were attached on slides and blocked with PBS that contained 1% bovine serum albumin (PBA) for 15 min. Then, samples were incubated with anti-β-tubulin mouse monoclonal (Sigma) for 1 h, followed by AlexaFluor 594-conjugated goat anti-mouse antibody (Molecular Probes, Eugene, OR) for 1 h. Slides were then washed in PBA, incubated with 0.5 mg mL^{-1} Hoechst 33341 (Sigma) for 5 min, mounted with Mowiol and examined by fluorescence microscopy (Leica).

Detection of apoptosis

Apoptosis was detected by terminal deoxynucleotidyl-transferase-mediated deoxyuridine triphosphate nick-end labelling (TUNEL assay). Cells were fixed in 4% paraformaldehyde for 45 min, at room temperature and processed according to the manufacturer's instructions of the in situ Cell Death Detection Kit Fluorescein (Roche, Mannheim, Germany) and the sample were analysed by flow cytometer (Becton Dickinson).

Tubulin assembly assay

Tubulin was purified from bovine brain that was purchased from a local slaughterhouse; the tubulin was conserved before use in ice-cold Pipes buffer (100 mM K-Pipes, pH 6.9, 2 mM EGTA, and 1 mM MgCl$_2$) and was used as soon as possible. Pure tubulin was obtained by two cycles of polymerisation–depolymerisation in a high-molarity buffer.[26] Stock solutions of compounds were prepared by dissolving the powders at a concentration of 2 mM in dimethyl sulfoxide. To assess the effect of the compounds on tubulin assembly in vitro, tubulin (2 mg mL^{-1}) was mixed with the compounds (0.1–100 μM) or vehicle in an assembly buffer (80 mM K-Pipes, pH 6.9, 2 mM EGTA, 1 mM MgCl$_2$, 1 mM GTP and 10% glycerol) and incubated at 37 °C for 30 min. At the end of polymerisation, unpolymerised and polymerised fractions of tubulin were separated by centrifugation at 30 000 g for 30 min at 30 °C. The relative amount of unpolymerised tubulin was 60 ± 4% of the total tubulin. The EC$_{50}$ was defined as the compound concentration that resulted in a 50% decrease in protein in the unpolymerised fraction relative to control reaction mixtures without the compound.[27] Protein con-

centration was determined by MicroBCA assay kit (Pierce, Rockford, IL, USA).

Computational details

Molecular modelling studies were conducted on a quad-Xeon workstation that was running Linux. The tubulin–substrate complex was constructed by docking the ligands into the equilibrated tubulin structure by using Autodock 3.0. Then the system was equilibrated with a series of minimisations interspersed by short molecular dynamics simulations. The resulting structure was used as the starting model for the 1 ns molecular dynamics simulation, and the structure that was obtained from molecular dynamics simulation was then optimised by using an AMBER force field.[28]

Conformational analysis and ligand preparation

The oxadiazole derivatives were submitted to a modelling study through theoretical calculations. The starting conformations of the ligands were optimised with quantum mechanical calculations by using Gaussian 03[29] (6-31g* base set[30]). The conformational space was explored by using the molecular dynamics module of TINKER.[31–33] Simulation in explicit water were performed at 298 K by using the AMBER force field in a $30 \times 30 \times 30$ box of standard TIP3P-equilibrated water models,[34–36] with a minimum solvent–solute distance of 2.3 Å, at constant temperature and pressure (Berendsen scheme,[37] bath relaxation constant 0.2). A 50 ps simulation at 1200 K was then used to generate 100 random structures that were subsequently subjected to a 20 ps restrained MD with a 50% scaled force field at the same temperature, followed by 20 ps at 1200 K with full restraints. The resulting molecular conformations were then optimised with respect to all the torsion angles, and convergence was assumed when the energy changes in two subsequent cycles of the minimisation procedure was <0.01 kcal mol^{-1}. For all compounds the resulting geometries of the thus-located minimum energy conformations were re-optimised by using the default scheme in Gaussian 03 at the B2LYP/6-31G(d) level of theory.[30] The solvation energy was calculated with continuum solvent models (C-PCM) to take into account the strong influence of water on the behaviour of these compounds. The structures that showed the lowest internal energy and the least number of violations of the experimental data were selected and analyzed. All ligands atomic charges were assigned by using the Gasteiger–Marsili formation, which is the type of atomic charges that are used in calibrating the AutoDock empirical free energy function.[38]

Preparation of the tubulin system

The starting model of the three-dimensional tubulin structure (PDB code: 1SA1) was obtained from the Protein Data Bank[39] and checked through DeepView[40] to guarantee the system conformity with the molecular modelling programs (in particular, the names of the side chains that must be congruent with the used force field). The amino acid chain of the tubulin model was terminated with COO^- and NH^{3+} groups in their zwitterionic form, and the polar hydrogen atoms were added in their calculated positions. The protonation state for all the ionisable residues was set to the normal ionisation state at pH 7.0, and both the topology and connectivity of the molecule were created. The system was then fully optimised up to an energy gradient that was lower than 10^{-4} kcal mol^{-1} Å. The preferred conformations that were adopted in water solution were used as the starting structure for the oxadiazole derivatives,

whereas that of podophyllotoxin was obtained from the original model (PDB code: 1SA1).

Molecular docking

To test the ability of the AutoDock[18–21] program to replicate the ligand binding to tubulin, the podophyllotoxin molecule was initially docked, and the orientation of the resulting lowest-energy structure was compared with the crystallographic structure. A near perfect superposition (RMSD: 0.60 Å) was obtained; this result demonstrated AutoDock's ability to locate the podophyllotoxin binding site in tubulin. To find binding regions of the oxadiazole derivatives into the tubulin structure, an automated docking simulation was implemented with the program AutoDock version 3.0. Atomic solvation parameters and fragmental volumes were assigned to the protein atoms by using the AutoDock utility, AddSol. All ligand atoms but no protein atoms were allowed to move during the docking simulation, and the rotatable bonds in the ligand were defined by using another AutoDock utility, AutoTors. The interaction energy between ligand and protein was evaluated by using atom affinity potentials that were precalculated on a grid. Because of the absence of information on the binding region for the ligands, the docking process was performed by using a two-step approach. In the first step, the docking procedure was applied to the whole α,β-tubulin dimer, without imposing any binding site, by using the so-called "blind docking" approach.[22, 23] A grid map of 30 Å in each x, y and z direction that was centred at the middle of the podophyllotoxin binding site was used. The resulting docked conformations were clustered into families of similar binding modes, with an RMSD clustering tolerance of 2 Å. In the second step, we docked the oxadiazole ligands in the binding sites that were found in the first step ("refined docking"). This time, a grid map of 7 Å in each *x*, *y*, and *z* direction was considered, with a grid resolution of 0.375 Å. The grid maps were calculated by using AutoGrid. Docking was performed by using the Lamarckian genetic algorithm in AutoDock 3.0. Each docking experiment was performed 100 times to yield 100 docked conformations. The parameters that were used for the docking were as follows: population size of 50; random starting position and conformation; maximal mutation of 2 Å in translation and 50 degrees in rotations; elitism of 1; mutation rate of 0.02 and crossover rate of 0.8; and local search rate of 0.06. Simulations were performed with a maximum of 1.5×10^6 energy evaluations and a maximum of 27 000 generations. The pseudo-Solis and Wets local search method was included with the default parameters. The final docked conformations were clustered by using a tolerance of 1 Å RMSD. The lowest docking-energy conformations were equilibrated for 1 ns by unrestrained MD. The simulations were performed by working at constant temperature and pressure (NPT ensemble) in a periodic cubic box of TIP3P water molecules. The bond distances and bond angles of water were constrained by using the SETTLE algorithm,[41] and the bond lengths within the protein were constrained with the LINCS algorithm.[42] The coupling time was set to 1.0 ps and the isothermal compressibility was set to 4.6×10^{-5} bar^{-1}. The tubulin, ligands and solvent were independently coupled to a temperature of 298 K with a coupling time of 0.1 ps and the pressure was held at 1 bar, with a coupling time of 0.2 ps by using a Berendsen thermostat to maintain the constant temperature and pressure. The time step that was used was 1.0 fs. Snapshots of the tubulin–substrate system were saved every 0.2 ps, and a total of 6000 snapshots were saved. Hydrogen bonds and contacts were automatically identified using contact module of CCP4,[43] while the other interactions were identified visually.

Acknowledgements

[1] R. Heald, E. Nogales, *J. Cell Sci.* **2002**, *115*, 3–4.

[2] E. Rowinsky, R. C. Donehower, *Cancer: Principles and Practice of Oncology*, 6th ed., **2001**, pp. 431–452.

[3] E. Hamel, *Med. Res. Rev.* **1998**, *18*, 259–295.

[4] H. Prinz, *Expert Rev. Anticancer Ther.* **2002**, *2*, 695–708.

[5] P. Giannakakou, R. Gussio, E. Nogales, K. H. Downing, B. Zaharevitz, B. Bollbuck, G. Poy, D. Sackett, K. C. Nicolaou, T. Fojo, *Proc. Natl. Acad. Sci. USA* **2000**, *97*, 2904–2909.

[6] a) J. Crown, M. O'Leary, *Lancet* **2000**, *355*, 1176–1178; b) E. K. Rowinsky, R. C. Donehower, *New Engl. J. Med.* **1995**, *332*, 1004–1014.

[7] a) R. B. G. Ravelli, B. Gigant, P. A. Curmi, I. Jourdain, S. Lachkar, A. Sobel, M. Knossow, *Nature* **2004**, *428*, 198–202; b) J. Löwe, H. Li, K. H. Downing, E. Nogales, *J. Mol. Biol.* **2001**, *313*, 1045–1057.

[8] D. W. Heinz, W. Schubert, G. Höfle, *Angew. Chem.* **2005**, *117*, 1324–1327; *Angew. Chem. Int. Ed.* **2005**, *44*, 1298–1301.

[9] B. H. Long, J. M. Carboni, A. J. Wasserman, L. A. Cornell, A. M. Casazza, P. R. Jensen, T. Lindel, W. Fenical, C. R. Fairchild, *Cancer Res.* **1998**, *58*, 1111–1115.

[10] G. Murineddu, G. Cignarella, G. Chelucci, G. Loriga, G. A. Pinna, *Chem. Pharm. Bull.* **2002**, *50*, 754–759.

[11] X. Ouyang, E. L. Piatnitski, V. Pattaropong, X. Chen, H. Y. He, A. S. Kiselyov, A. Velankar, J. Kawakami, M. Labelle, L. Smith II, J. Lohman, S. P. Lee, A. Malikzay, J. Fleming, J. Gerlak, Y. Wang, R. L. Rosler, K. Zhou, S. Mitelman, M. Camara, D. Surguladze, J. F. Doody, M. C. Tuma, *Bio. Med. Chem. Lett.* **2006**, *16*, 1191–1196.

[12] P. Perego, M. Giarola, S. C. Righetti, R. Supino, C. Camerini, D. Delia, M. A. Pienotti, T. Miyashita, J. C. Reed, F. Zunino, *Cancer Res.* **1996**, *56*, 556–562.

[13] M. V. Blagosklonny, P. Giannakakou, W. S. El-Deiry, D. G. Kingston, P. I. Higgs, L. Neckers, T. Fojo, *Cancer Res.* **1997**, *57*, 130–135.

[14] Y. H. Ling, C. Tornos, R. Perez-Soler, *J. Biol. Chem.* **1998**, *273*, 18984–18991.

[15] C. Vogel, A. Kienitz, I. Hofmann, R. Müller, H. Bastians, *Oncogene* **2004**, *23*, 6845–6853.

[16] D. W. Meek, *Pathol. Biol.* **2000**, *48*, 246–254.

[17] Y. Zhang, N. Li, C. Caron, G. Matthias, D. Hess, S. Khochbin, P. Matthias, *EMBO J.* **2003**, *22*, 1168–1179.

[18] D. S. Goodsell, A. J. Olson, *Proteins* **1990**, *8*, 195–202.

[19] G. M. Morris, D. S. Goodsell, R. Huey, A. J. Olson, *J. Comput.-Aided Mol. Des.* **1996**, *10*, 293–304.

[20] G. M. Morris, D. S. Goodsell, R. S. Halliday, R. Huey, W. E. Hart, R. K. Belew, A. J. Olson, *J. Comput. Chem.* **1998**, *19*, 1639–1662.

[21] AutoDock version 3.0.5: http://autodock.scripps.edu/ (accessed February 20, 2009).

[22] C. Hetényi, D. van der Spoel, *Protein Sci.* **2002**, *11*, 1729–1737.

[23] C. Hetényi, D. van der Spoel, *FEBS Lett.* **2006**, *580*, 1447–1450.

[24] P. Perego, M. De Cesare, P. De Isabella, N. Carenini, G. Beggiolin, G. Pezzoni, M. Palumbo, L. Tartaglia, G. Pratesi, C. Pisano, P. Carminati, G. LScheffer, F. Zunino, *Cancer Res.* **2001**, *61*, 6034–6037.

[25] V. Zuco, C. Zanchi, C. Lanzi, G. L. Beretta, R. Supino, C. Pisano, M. Barbarino, R. Zanier, F. Bucci, C. Aulicino, P. Carminati, F. Zunino, *Neoplasia* **2005**, *7*, 667–677.

[26] M. Castoldi, A. V. Popov, *Protein Expression Purif.* **2003**, *32*, 83–88.

[27] M. D. Chordia, D. G. I. Kingston, E. Hamel, C. M. Lin, B. H. Long, C. A. Fairchild, K. Johnston, W. C. Rose, *Bioorg. Med. Chem.* **1997**, *5*, 941–947.

[28] W. D. Cornell, P. Cieplak, C. I. Bayly, I. R. K. M. Gould, Merz, D. M. Ferguson, D. C. Spellmeyer, T. Fox, J. W. Caldwell, P. A. Kollman, *J. Am. Chem. Soc.* **1995**, *117*, 5179–5197.

[29] M. J. Frisch, G. W. Trucks, H. B. Schlegel, G. E. Scuseria, M. A. Robb, J. R. Cheeseman, J. A. Montgomery, T. Vreven, K. N. Kudin, J. C. Burant, *Gaussian 03, Revision A.1*, **2003**, Gaussian, Pittsburgh, PA (USA).

[30] W. Hehre, L. Radom, P. Schleyer, J. Pople, *Ab Initio Molecular Orbital Theory*, **1986**, John Wiley, New York, NY (USA).

[31] P. Ren, J. W. Ponder, *J. Phys. Chem. B* **2003**, *107*, 5933–5947.

[32] R. V. Pappu, R. K. Hart, J. W. Ponder, *J. Phys. Chem. B* **1998**, *102*, 9725–9742.

[33] Y. Kong, J. W. Ponder, *J. Chem. Phys.* **1997**, *107*, 481–492.

[34] H. J. C. Berendsen, J. P. M. Postma, W. F. van Gunsteren, J. Hermans, *Intermolecular Forces* **1981**, 331–342.

[35] W. L. Jorgensen, J. Chandrasekhar, J. Madura, R. W. Impey, M. L. Klein, *J. Chem. Phys.* **1983**, *79*, 926–933.

[36] E. Lindahl, B. Hess, D. van der Spoel, *J. Mol. Model.* **2001**, *7*, 306–317.

[37] H. J. C. Berendsen, J. P. M. Postma, W. F. van Gunsteren, A. DiNola, J. R. Haak, *J. Chem. Phys.* **1984**, *81*, 3684–3690.

[38] J. Gasteiger, M. Marsili, *Tetrahedron* **1980**, *36*, 3219–3228.

[39] http://www.rcsb.org (accessed February 20, 2009).

[40] http://expasy.org/spdbv/ (accessed February 20, 2009).

[41] S. Miyamoto, P. A. Kollman, *J. Comput. Chem.* **1992**, *13*, 952–962.

[42] B. Hess, H. Bekker, H. J. C. Berendsen, J. G. E. M. Fraaije, *J. Comput. Chem.* **1997**, *18*, 1463–1472.

[43] Collaborative Computational Project No. 4, *Acta Crystallogr. D* **1994**, *50*, 760–763.

FULL PAPERS

Antitumour activity was observed in a series of tricyclic compounds characterised by a 2-(1H-pyrrol-3-yl)-1,3,4-oxadiazole moiety with various substitutions. Their synthesis and antiproliferative activity toward a panel of human tumour cell lines is described. The most interesting compounds **1 c** and **4 c** were selected for further evaluation to elucidate their possible mechanism of action.

X = CH₂ (**1**); (CH₂)₂ (**2**); (CH₂)₃ (**3**); CH=CH (**4**)
R = H (**a**), CH₃ (**b**), C₆H₅ (**c**)
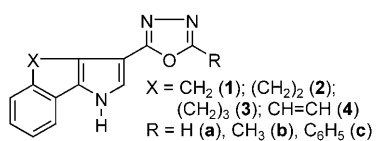
G. A. Pinna, G. Murineddu, C. Murruzzu, V. Zuco, F. Zunino, G. Cappelletti, R. Artali, G. Cignarella, L. Solano, S. Villa*

■■ – ■■

Synthesis, Modelling, and Antimitotic Properties of Tricyclic Systems Characterised by a 2-(5-Phenyl-1H-pyrrol-3-yl)-1,3,4-oxadiazole Moiety

These are not the final page numbers! ↗↗